Chapter 16
Au Electrocatalysis for Oxygen Reduction

Francisco J. Vidal-Iglesias, José Solla-Gullón, Enrique Herrero, and Juan M. Feliu

Abstract This chapter reviews the recent advances on the study of the oxygen reduction reaction (ORR) on gold electrodes. The initial part is devoted to the study of the reaction on single-crystal electrodes to determine the effect of the surface structure on the reactivity of gold electrodes for this reaction. The best reactivity is found for the Au(100) electrode in alkaline medium. For the nanoparticle electrodes, the reactivity for this reaction depends on two different effects: size and surface structure effects. Regarding the size effects, the different studies found in the literature do not agree on whether the size of the nanoparticles has a significant impact on the reactivity for the ORR. This disagreement between different authors is probably due to the lack of control of the surface structure of the nanoparticles. On the other hand, significant effects are found when the surface of the nanoparticle is changed. In general, the reactivity in alkaline media increases as the fraction of {100} domains on the surface increases. In some cases, the reactivity of gold in alkaline medium is similar to that measured for platinum electrodes.

16.1 Introduction

It is clear that the oxygen reduction reaction (ORR) is one of the most important electrochemical reactions since it has multiple applications. The potential fields range from the energy conversion to corrosion science. For this reason, it has been the subject of numerous works throughout the years. In the complete reduction of oxygen to water, there are four electrons exchanged. This high number of electrons

F.J. Vidal-Iglesias • J. Solla-Gullón • E. Herrero (✉) • J.M. Feliu (✉)
Instituto de Electroquímica, Universidad de Alicante, Apdo. 99, 03080 Alicante, Spain
e-mail: herrero@ua.es; juan.feliu@ua.es

M. Shao (ed.), *Electrocatalysis in Fuel Cells*, Lecture Notes in Energy 9,
DOI 10.1007/978-1-4471-4911-8_16,

exchanged necessarily implies existence of several intermediates. Since the reaction is sensitive to the nature of the electrode, at least one of the intermediates (if not all) should be adsorbed on the electrode surface. Thus, nature and surface structure of the electrode is a fundamental aspect to consider when the ORR is studied. Among pure metals, platinum is recognized as the electrode with the highest electrocatalytic activity [1].

The substrate not only affects the electrocatalytic activity but also the final product of the reaction and the mechanism. The general mechanism for oxygen reduction consists in two interconnected parallel pathways: the first leading to the formation of water (OH^- in basic media) with hydrogen peroxide (HO_2^- in basic media) as intermediate species and the second path yielding water (OH^- in basic media) directly [2, 3]. Depending on the metal, the final product can be water (OH^-) or hydrogen peroxide. In these latter cases, the further reduction of hydrogen peroxide is highly inhibited.

In the case of gold electrodes, the general mechanism for the ORR [1] can be simplified as follows for the reactions in acid medium:

$$O_2 + 4H^+ + 4e \rightleftharpoons 2H_2O$$

$$O_{2,b} \xrightarrow{dif} \boxed{O_{2,a} \xrightarrow[H^+]{1e^-} HO_{2,a}} \xleftrightarrow[H^+]{1e^-} H_2O_{2,a} \xleftrightarrow[H^+]{1e^-} OH_a + H_2O \xleftrightarrow[H^+]{1e^-} 2H_2O$$

$$H_2O_{2,a} \updownarrow H_2O_{2,b}$$

where the subscript "a" denotes an adsorbed species and "b" a bulk species. When the reaction occurs in alkaline medium, the mechanism is transformed into

$$O_2 + 2H^+ + 4e \rightleftharpoons 2OH^-$$

$$O_{2,b} \xrightarrow{dif} \boxed{O_{2,a} \xrightarrow{1e} O_{2,a}^-} \xleftrightarrow[H^+]{1e} HO_{2,a}^- \xleftrightarrow{1e} O_a^- + OH^- \xleftrightarrow[H^+]{1e} 2OH^-$$

$$HO_{2,a}^- \updownarrow HO_{2,b}^-$$

In this chapter, recent results on the oxygen reduction reaction will be covered. We will focus on the results obtained with gold nanoparticles. However, some results obtained with single-crystal electrodes will be presented since they are necessary to understand the results found for the nanoparticle electrodes. Although the mean electrocatalytic activity of the gold electrode is lower than that of platinum, Au(100) electrode in alkaline medium has a similar activity for the ORR than platinum, and for that reason, it has been studied systematically and abundantly.

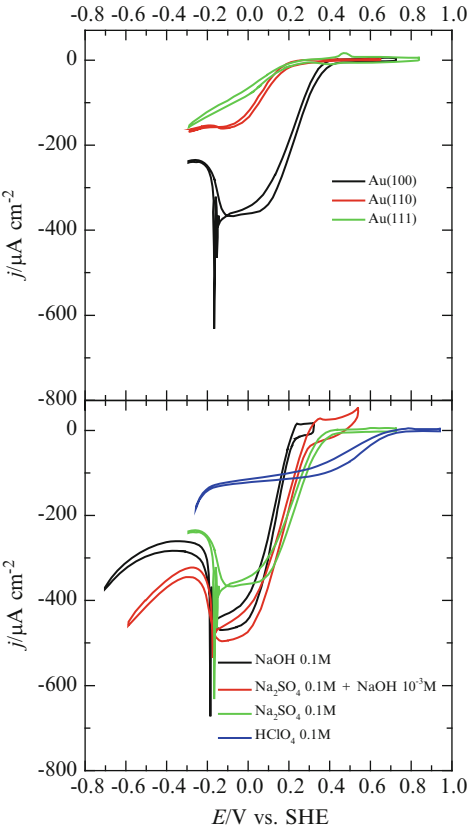

Fig. 16.1 *Top panel*. Current densities measured for oxygen reduction in the impinging jet system in 0.1 M Na_2SO_4 (pH = 6) for the Au (100), Au(111), and Au(110) electrodes. *Bottom panel*. Effect of the pH in the oxygen reduction in the impinging jet system for the Au(100) electrode

16.2 ORR in Gold Single Crystals

The electrocatalytic activity of gold electrodes for the ORR is not very high. The first studies carried out in acid medium with Au single crystals showed that the reaction was structure sensitive, but the onset for the ORR was ca. 400 mV more negative than those measured in equivalent conditions for platinum [4, 5]. Additionally, the number of electrons transferred in the reaction was two, indicating that the final product was hydrogen peroxide. In fact, the reduction of hydrogen peroxide was highly inhibited and only took place at potentials close to hydrogen evolution.

When the same experiments were carried out in neutral and alkaline media, the voltammetric behavior showed significant differences for some electrodes. The Au(111) and Au(110) electrodes exhibited a similar behavior to that observed in acid medium. However, the onset for the ORR on the Au(100) electrode was displaced significantly to more positive potentials, with an electrocatalytic activity similar to that of platinum (Fig. 16.1) [6–13]. Additionally, four electrons were exchanged at high potentials, whereas a change in mechanism took place at lower potential and only hydrogen peroxide was formed. In parallel with this behavior, the Au(100)

electrode exhibited a significant activity for the reduction of hydrogen peroxide in the same region where the four-electron mechanism is operative [6, 9]. In the transition between the two- and four-electron mechanisms, oscillations can be observed [9, 13]. The oscillations are linked to the appearance of the inhibition of the reaction at lower potentials, which corresponds to a negative resistance in the equivalent that compensates the solution resistance [14].

The studies with stepped surfaces revealed that the enhanced electrocatalytic activity for the ORR in alkaline solutions is exclusively linked to the presence of {100} bidimensional domains [10, 12, 15, 16]. However, the origin of the high catalytic activity of these domains for the ORR is still not clear. Adzic and col. attributed the differences to the different OH adsorption properties of the domains [15]. In summary, it has been proposed that adsorbed OH catalyzes the cleavage of the O–O bond in the peroxide and leads to the transfer of four electrons [10, 17]. However, the voltammetric profiles of the different electrodes show similar OH adsorption properties in the region where the oxygen reduction takes place [13]. Thus, it was proposed that different behavior for the ORR should be related to structural differences. Additionally, the transition between the two- and four-electron mechanism takes place at a constant potential, which also suggests that OH adsorption is not responsible for the catalytic enhancement of the ORR on the Au(100) electrode [13]. Some experiments have suggested the presence of adsorbed HO_2^- in alkaline medium on gold electrodes and attributed a very important role in the mechanism to this species [18]. Also DFT studies indicate that adsorbed OOH, rather than O_2, is the most important intermediate which determines the final outcome of the reduction process [19]. Other studies propose that the Au(100)–O_2 interaction and the number of sites available for the reduction of oxygen controls the reaction rate [20].

The previous discussion/introduction summarizes the knowledge of electrocatalytic properties of Au single crystals toward ORR. Nevertheless, it is well known that for practical purposes, the use of the catalysts in the form of nanoparticles of dimensions as small as possible is required. In these nanoparticles the surface over volume ratio is maximized and consequently the amount of catalyst is minimized, thus reducing costs associated with their use in large-size/scale applications. In addition, it is well established that the electrocatalytic properties of a nanoparticle are mainly determined by the electronic properties of the surface atoms which in turn depend on a set of physical parameters that include chemical composition (at surface and bulk), particle size, and particle shape/surface structure. In principle, one could tailor their properties by controlling any of those parameters to optimize the activity of the catalyst for a particular reaction. Thus, and because the aim of this chapter is to review the electrocatalysis of gold toward ORR, the chemical composition of the nanoparticles is defined (gold), and therefore in the following sections, we will summarize and discuss the most relevant contributions related to the effect of the particle size and particle shape/surface structure for gold nanostructures toward ORR.

16.3 Effect of Particle Size

The electrocatalytic properties defined as the current density per active area measured at given potential should be in principle independent of the size of the nanoparticles. However, the diminution of size could lead to changes in the reactivity due to two main factors: (1) if the number of atoms in the nanoparticle is too small, the band structure of the metal is not completely developed and the electronic properties may differ significantly from that observed for bulk gold and (2) the ratio of atoms with low-coordination number in the surface, which are regarded generally as more reactive, increases with the diminution of the size. For that reason, below a certain size (ca. 4–7 nm), different electrocatalytic activities can be found for the nanoparticles. Thus, the effect of the nanoparticle size has been extensively studied.

One of the first contributions related to the effect of the particle size for oxygen reduction on gold was reported by Sarapuu et al. [21]. They investigated the influence of the loading of evaporated gold on the kinetics of the ORR at thin-film gold electrodes in acid electrolyte (0.5 M H_2SO_4) and compared their behavior with bulk gold with the main objective of evaluating the influence of the particle size in the ORR. They observed that the kinetics of O_2 reduction on the electrodes, including specific activity, Tafel slope, and n (number of transferred electrons) value, were almost independent of the film thickness (thickness between 0.25 and 50 nm) and similar to those observed with a bulk gold electrode, thus suggesting the absence of a particle size dependence. However, subsequent contributions by El-Deab and Ohsaka [22] and Zhang et al. [23] observed remarkably high electrocatalytic activities toward oxygen reduction in acidic solutions with electrochemically deposited Au nanoparticles on polycrystalline Au and boron-doped diamond (BDD) electrodes, respectively. El-Deab and Ohsaka [22] reported that for gold nanoparticles electrodeposited on gold electrodes, the ORR in 0.5 M H_2SO_4 solution showed two well-defined reduction peaks at +50 and −250 mV versus Ag/AgCl. This behavior was remarkably different from that observed with the bare gold electrode in which only a reduction peak was observed at −200 mV. They attributed these two reduction peaks at the gold nanoparticles as a two-step four-electron reduction pathway of O_2 in which the peak at more positive potential was due to the two-electron reduction of O_2 to H_2O_2, whereas that at lower potentials was assigned to the further reduction of H_2O_2 to H_2O. This behavior was clearly different from that found with the bulk gold electrode, at which only the two-electron reduction peak of O_2 to H_2O_2 was observed. The proposed mechanism was verified by performing similar ORR experiments in presence of 2.3 mM H_2O_2 solution resulting in an evident increase in the reduction peak current related to the reduction of H_2O_2 to H_2O, while the reduction peak current associated with the reduction of O_2 to H_2O_2 remained almost unaltered. Interestingly, they also observed that the increase of the particle size resulted in a clear loss of the activity of the two-electron reduction of O_2 to H_2O_2 (Fig. 16.2).

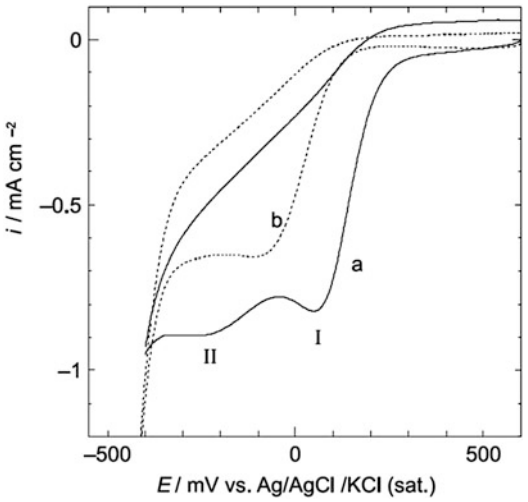

Fig. 16.2 CVs obtained for the O_2 reduction at Au nanoparticle-deposited Au electrodes in O_2-saturated 0.5 M H_2SO_4. A potential step from 1.1 to 0 V was used for the electrodeposition of Au particles from 0.5 M H_2SO_4 solution containing 0.11 mM $Na[AuCl]_4$ with deposition time of (a) 5 s and (b) 10 s. Potential scan rate = 100 mV s^{-1} (extracted from [22])

In a later work, and using the RDE, they also observed [24] that the number of electrons involved in the electrochemical reduction of O_2 was about 4 for the Au nanoparticle-electrodeposited electrode and 3 for bulk Au electrode at the same potential (−350 mV vs. Ag/AgCl/KCl(sat.)) (Fig. 16.3), thus indicating a higher reduction and decomposition of H_2O_2 at the gold nanoparticles. In addition, the reported Tafel slopes for both systems (the nanoparticles and bulk gold electrode) were similar, suggesting that the O_2 reduction at both electrodes proceeds by a similar mechanism. However, they also observed that the kinetic current of the gold nanoparticles was higher than that of the bulk Au electrode at the same potential.

Similarly, Zhang et al. [23] reported that the O_2 reduction rate on the Au nanoparticles (~60 nm) deposited on BDD was 20 times higher than that of bulk Au electrode. In addition, they also observed that the reaction mechanism of oxygen reduction was modified from a two-electron reduction to a four-electron reduction in the potential range of −200 to −400 mV versus SCE at the Au nanoparticle-deposited BDD. However, when similar experiments were performed in alkaline (0.1 M KOH) or in neutral (0.1 M phosphate buffer solution ~ pH 7.2) solutions, such enhanced activity toward ORR was not clearly observed [25, 26].

When the electrocatalysis of the ORR was studied on gold nanoclusters deposited by vacuum evaporation on a BDD electrode in 50 mM H_2SO_4 solution, Yagi et al. observed that the ORR activity was again influenced by the particle size [27]. Thus, the electrode with 3 nm nanoparticles was the most active. Unfortunately, as authors stated, the size dispersions of the samples were quite broad and the optimum particle size for oxygen reduction could not be determined. However, the activity of the samples was significantly higher than that at a polycrystalline gold electrode, and a clear positive shift of the O_2 reduction peak toward positive potentials and an increase in the current efficiency consumed for the four-electron reduction were observed. In addition, a two-step four-electron reduction pathway of

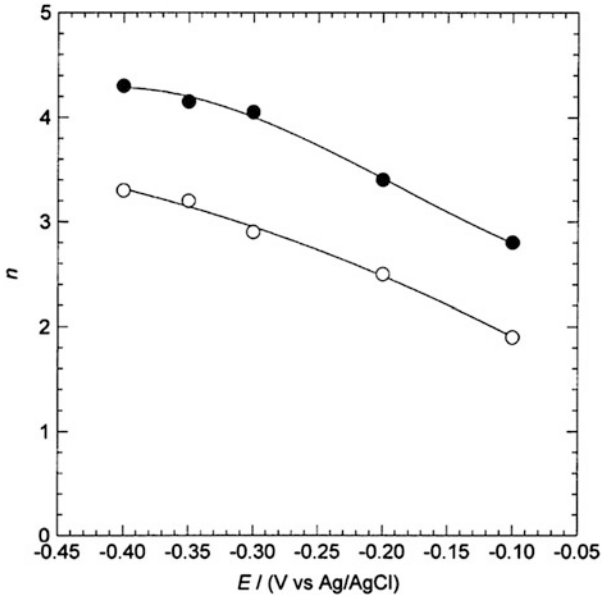

Fig. 16.3 Dependence of n on the potential for O_2 reduction at (*open circles*) bulk and (*filled circles*) Au nanoparticle-electrodeposited Au electrodes (extracted from [24])

O_2 to H_2O at the Au nanoparticles was directly proved by a four-electrode configuration. Also, they observed that after a heat treatment (600 °C under H_2 atmosphere) of the samples, the electrocatalytic activity improved, which was attributed to a modification of the particle shape and consequently with a modification of the crystallographic orientations exposed at the surface of the nanoparticles.

In good agreement with Yagi et al., Guerin et al. observed that for gold nanoparticles supported on substoichiometric titanium dioxide (TiO_x) and on carbon, the activity decreased for diameters <3 nm with decreasing particle size, independently of the supporting material [28]. Nevertheless, unlike the aforementioned studies, the catalytic activity was clearly independent of particle size above this critical size (Fig. 16.4).

In contrast with some of the previous observations, Bron observed that the ORR in acidic electrolyte solution at various Au/C catalysts with different support materials (VULCAN XC72 and Black Pearls) and different gold particle sizes between 2.7 and 42 nm [29] was neither dependent on the particle size nor on the supporting material. In addition, he found Tafel slopes around 105 mV and an average number of electrons transferred per oxygen molecule between 2 and 3, finding also that both parameters were independent on the gold particle size. From these results, he concluded that the oxygen reduction on carbon-supported gold catalysts is structure insensitive for particle sizes up to 2.7 nm.

In the same way, Sarapuu et al. [30] extended their previous works studying the ORR on nanostructured gold electrodes both in acidic (0.5 M H_2SO_4) and alkaline

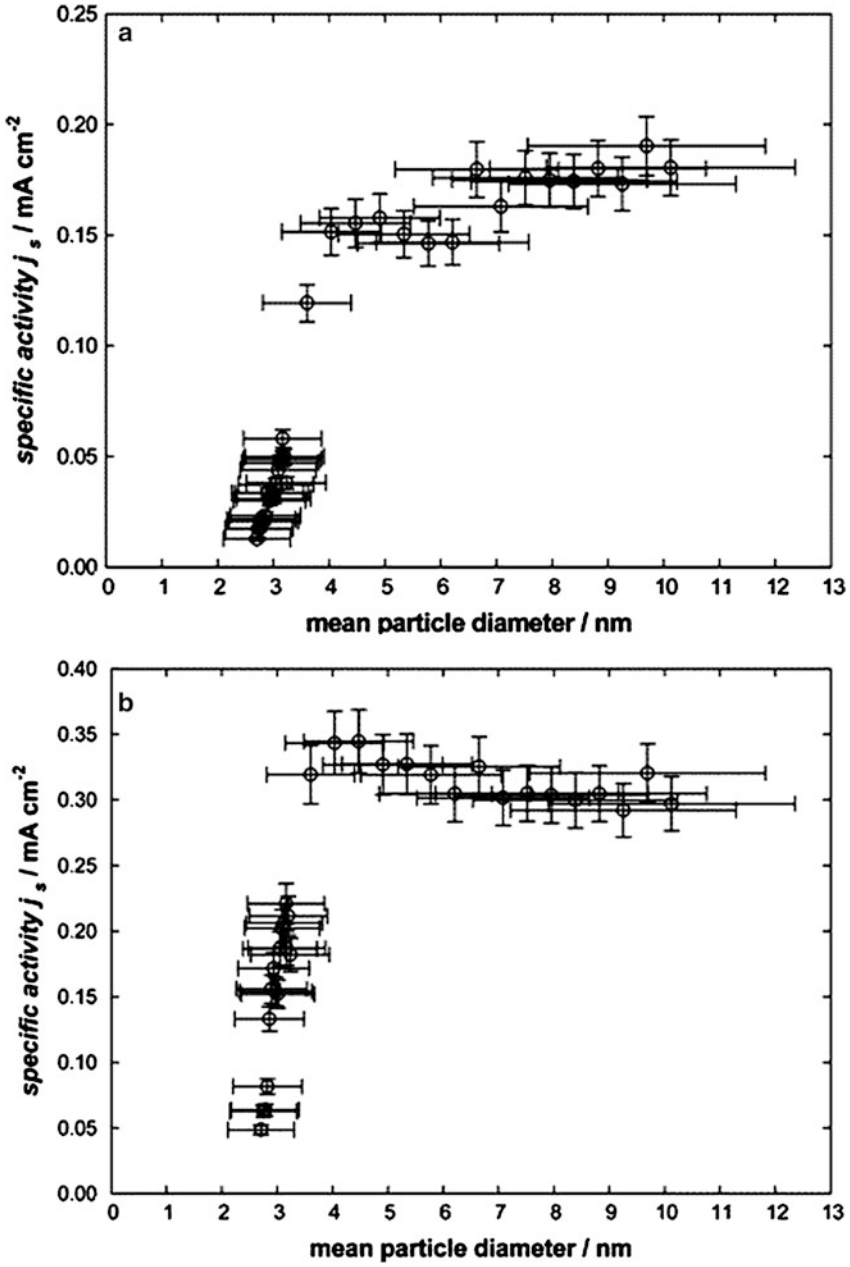

Fig. 16.4 Specific oxygen reduction activity of carbon-supported gold particles at (**a**) 0.40 V and (**b**) 0.30 V versus RHE measured on the (10 × 10) array of electrodes. The *error bars* along the particle size axis indicate the range of particle size (in fact, the standard deviation of the particle size) observed by TEM. The *error bars* on the specific activity axis reflect the standard deviation of the currents measured at the 10 electrodes on the array with a mean particle size (extracted from [28])

(0.1 M KOH) media. Thin films of gold surfaces, with a nominal thickness of 0.25–20 nm, were prepared by vacuum evaporation onto glassy carbon (GC) electrodes and coated with a Nafion film. The Au particle size was clearly dependent on the loading of gold and varied from 2.7 ± 1.0 nm for a nominal thickness of 0.25 nm to 16 ± 6 nm corresponding to 20 nm nominal thickness. In agreement with their previous findings, they again observed that the Tafel slopes were close to −120 mV for all electrodes in both solutions, indicating that the O_2 reduction mechanism is the same for thin film as for bulk Au electrodes. In addition, the specific O_2 reduction activity (SA) of the nanostructured Au electrodes in 0.5 M H_2SO_4 was almost constant over the range of Au thicknesses studied, whereas in 0.1 M KOH, the SA slightly decreased with decreasing film thickness. However, it is important to point out that the average SA values were approximately three times lower (0.14 ± 0.03 mA cm^{-2}) than those obtained with Au films in the absence of Nafion (SA = 0.43 ± 0.05 mA cm^{-2}) [21]. This evidence was attributed to a decrease in the number of reaction sites by Nafion, as proposed by Maruyama et al. who studied the effect of fluorinated alcohols on the kinetics of the ORR on bulk Au electrodes [31, 32]. A similar decrease of the kinetic current was also reported on Nafion-coated GC electrodes as compared to bare GC which was related to the lower pH at Nafion-coated GC and/or to blocking by the side chains of the Nafion polymer.

Subsequent studies by Tang et al. [33] suggested a strong size effect. They analyzed the dependence of the kinetics of the ORR in alkaline solution (0.5 M KOH) with the particle size of gold nanoparticles (3 and 7 nm) supported on carbon (Fig. 16.5). They observed that the ORR activity (kinetic current density, j_k) of the 3 nm gold nanoparticles was 2.5 times higher than that obtained with the 7 nm gold nanoparticles (3.5 vs. 1.5 mA cm^{-2} measured at −0.6 V vs. Ag/AgCl). In addition, a two-electron reduction was obtained with the 7 nm, whereas in case of the 3 nm, a four-electron reduction was observed. This unusual four-electron transfer obtained with the 3 nm Au nanoparticles was speculatively explained due to the high density of low-coordination sites on the 3 nm nanoparticles that may increase the activation of the peroxide intermediate, facilitating further reduction to water. Very interestingly, from experiments at different temperatures, they estimated the apparent activation energy for the 3 nm particles that was found to be half that of the 7 nm particles (0.1 and 0.2 eV, respectively). They proposed that the presence of a high fraction of surface sites with low-coordination atoms together with the decreased electrophilicity of the 3 nm Au nanoparticles results in an increase in the O–Au bond energy with a corresponding decrease in the activation energy of the critical step of molecular oxygen dissociative chemisorption, thus accelerating the rate-limiting step for oxygen reduction.

Likewise, Inasaki and Kobayashi [34] studied the influence of the particle size of Au nanoparticles on the kinetics of ORR in acidic solution (0.5 M H_2SO_4) and found a size effect. They prepared carbon-supported Au nanoparticles with different particle size (1.7 ± 0.5, 4.8 ± 2 and 13.2 ± 2 nm) and evaluated their electrocatalytic activity toward ORR together with that of a bulk Au electrode (Fig. 16.6). The results obtained showed a clear dependence of the ORR activity

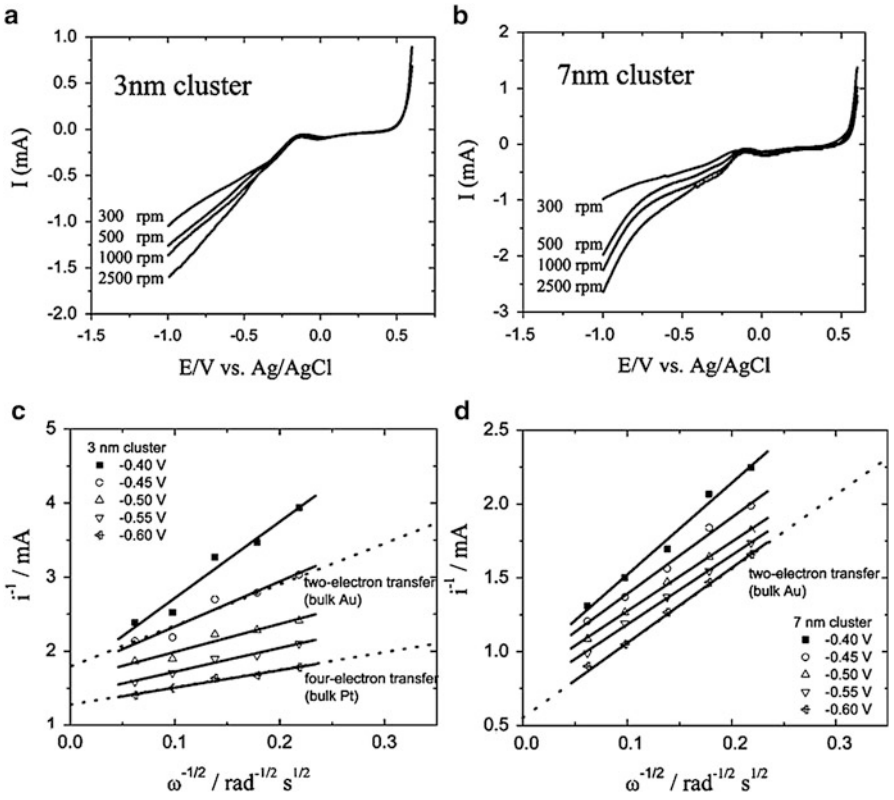

Fig. 16.5 Oxygen electroreduction on 3 and 7 nm Au nanoclusters in oxygen-saturated 0.5 M KOH. Cyclic voltammograms (sweep rate 10 mV s^{-1}) of Au nanoparticles on carbon rotating disk electrodes at several rotation speeds: (**a**) 3 and (**b**) 7 nm clusters. Levich plots of the voltammogram data (the currents at −0.6 V were used): (**c**) 3 and (**d**) 7 nm clusters (extracted from [33])

with the particle size. In detail, they reported that whereas for bulk gold, the number of electrons involved in the ORR was 2 and nearly constant at potentials above −0.2 V, for the nanoparticles, the n values increased as the potential became more negative and reached values of 2.3, 2.6, and 3.0 at −0.2 V versus Ag/AgCl for particles sizes of 1.7, 4.8, and 13 nm, respectively. These findings suggested that for smaller particle size, a two-step four-electron reduction or the direct four-electron reduction of O_2 to H_2O was favored.

Erikson et al. [35] also reported ORR results obtained with carbon-supported Au nanoparticles in 0.5 M H_2SO_4 and 0.1 M KOH solutions. They used commercial Au catalysts with different metal loading, 20 and 30 wt%, which also resulted in a different particle size, 11.0 ± 1.7 nm for 20 wt% catalyst and 14.0 ± 1.7 nm for 30 wt% catalyst. Nevertheless, in agreement with some of their previous studies, they concluded that the oxygen reduction activity of both carbon-supported Au

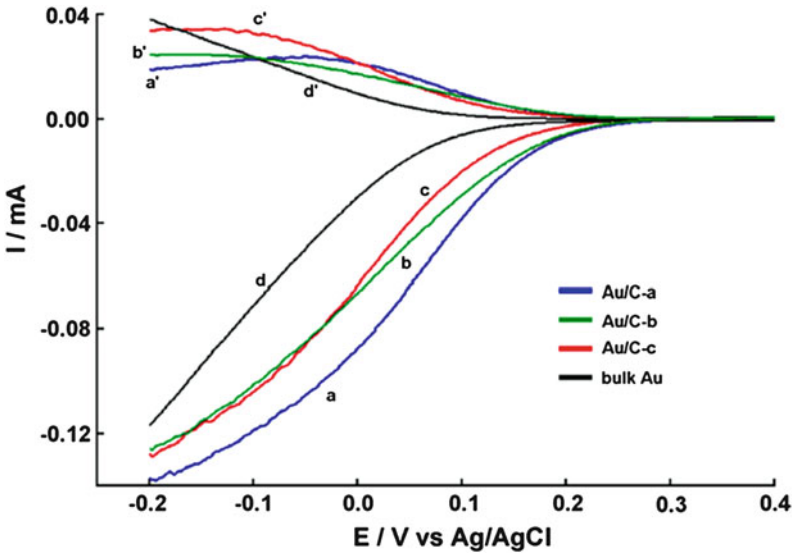

Fig. 16.6 RRDE voltammograms for the oxygen reduction in O_2-saturated 0.5 M H_2SO_4, at (a) (1.7 nm), (b) (4.8 nm), and (c) (13.2 nm) Au/C-modified GC electrodes and (d) bulk Au electrode at a rotation rate of 500 rpm. Curves a′–d′ represent the corresponding Pt-ring currents (polarized at 1.0 V). For the Au/C-modified electrodes, loading of Au metal on a GC electrode was fixed at 0.45 μg/electrode. $\nu = 10$ mV s^{-1} (extracted from [34])

nanoparticles was similar to the activity of bulk Au, both in acid and alkaline solutions. In addition, they also observed that the specific activity of Au was independent of the thickness of the catalyst layers, between 1.5 and 10 μm, indicating that the diffusion of O_2 within the layer was not affecting the results. In addition, they reported that the number of electrons involved in the reaction and the Tafel slopes were similar to those of bulk polycrystalline gold, which implies that the mechanism of O_2 reduction is not affected by the particle size.

The activity of very small nanoparticles has also been studied. Chen and Chen [36] prepared a series of Au nanoclusters with 11–140 gold atoms in the cores, corresponding to 0.8–1.7 nm in diameter, and performed ORR studies in alkaline medium to evaluate the size effect on the ORR electrocatalytic activity. Clear size dependence was observed in (1) the limiting current densities, increasing with decreasing core size; (2) the onset potential for ORR shifted to negative potential values with increasing Au cluster size; and (3) the kinetic current density increased with decreasing particle cores. Also, the oxygen reduction reaction was found to proceed by the efficient four-electron reaction pathway with the smaller clusters (Au_{11}, Au_{25}, and Au_{55}), whereas incomplete reduction occurred with the largest one (Au_{140}), for which the two-electron reaction route was favored.

In all these studies regarding the size effect in the ORR on gold electrodes, a general problem is the size distribution. The electrochemical response is always a macroscopic property which depends on the individual contributions of the different

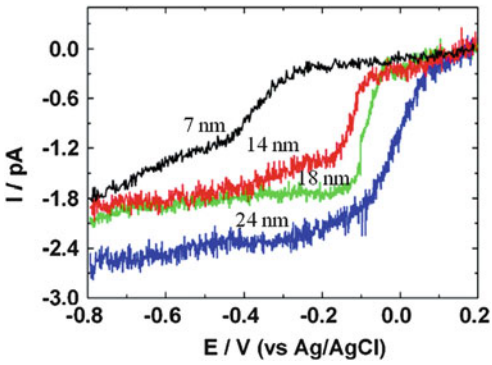

Fig. 16.7 Voltammetric responses of an oxygen-saturated 0.10 M KOH solution using a bare 7 nm diameter Pt nanoelectrode, a 14 nm Au SNPE, an 18 nm Au SNPE, and a 24 nm Au SNPE. The scan rate was 10 mV s (extracted from [37])

nanoparticles in the sample. In order to understand the effects of the size in the reaction, it would be important to address the reactivity of a single nanoparticle, as has been done using innovative methods by Li et al. [37]. In this study, they were able to immobilize a single Au nanoparticle at a SiO_2-encapsulated Pt disk nanoelectrode, previously oxidized and silanized. In such a system, the ORR in alkaline medium (0.1 M KOH solution) was studied. The Au single-nanoparticle electrode (SNPE) provided a larger diffusion-limited steady-state current than the one obtained with the bare Pt nanoelectrode. The Au nanoparticle exhibited a one-step process instead of a two-step pathway, similarly to the behavior of the bare Pt nanoelectrode for the ORR in alkaline medium. Moreover, the half-wave potential for the ORR at the Au SNPE was shifted toward higher potentials. The electrocatalytic activity for the ORR was also compared with Au nanoparticles of different sizes (14, 18, and 24 nm) and shown in Fig. 16.7. The steady-state limiting current increased with increasing the size of the Au nanoparticles, being 1.0, 1.7, and 2.0 pA for the 14, 18, and 24 nm Au nanoparticles, respectively. In addition, the half-wave potential at larger Au nanoparticles was also shifted to higher potentials, indicating higher catalytic activity. The half-wave potentials shifted from −365 mV versus Ag/AgCl at the bare Pt nanoelectrode to −130, −75, and −35 mV at the 14, 18, and 24 nm samples, respectively. These results clearly evidence a good Au size-dependent electrocatalytic activity toward ORR.

In some studies, the higher activity for the nanoparticle samples was credited to a lower contamination of the surface and/or the presence of higher number of low-coordinated atoms. Thus, Lee et al. [38] obtained the electrocatalytic properties for ORR in alkaline medium (0.5 M KOH solution) of carbon-supported Au nanoparticles with controlled particle size (3, 6, and 8 nm). The activity of these samples was compared with that obtained with commercial 5 and 10 nm Au nanoparticles. In all cases, the activity of the samples was higher than that of the commercial ones, which was attributed to the effectively cleaning and to the higher degree of disorder on the surfaces. However, the most active Au samples were those having 8 nm particle size, even when the currents were normalized by the weight of Au NPs, which is, from our point of view, quite unexpected.

Also, the surface structure effects were found in the study by Alexeyeva et al. [39]. They reported the analysis of the ORR on Au nanoparticles deposited on

multiwalled carbon nanotubes (MWCNTs). The carbon nanotubes were decorated with Au nanoparticles using a magnetron-sputtering technique. The sample was heat-treated and they found that by varying the annealing temperature it was possible to modify the morphology of Au nanoparticles thus allowing correlating their morphology with their electrocatalytic activity toward the ORR in acidic solution (0.5 M H_2SO_4). They showed an optimal temperature of 300 °C which was proved to be beneficial to ensure a larger active surface area and increased electrocatalytic activity. This sample consisted of regularly shaped rounded Au nanoparticles with a mean particle size of 11 nm. However, a high Tafel slope value was observed at low overpotentials (−200 mV), far from the typical slope value for O_2 reduction on gold in acid solution (−120 mV), corresponding to the slow transfer of the first electron to O_2 molecule. The reasons for this high Tafel slope remain still unclear.

In the same way, Jirkovsky et al. [40] used carbon-supported Au nanoparticles of mean size between 4.2 and 9.5 nm and studied the dependence of the ORR on nanoparticle size. Their findings suggested particle size dependence and showed a maximum electrocatalytic activity at a particle size of 5.7 nm from which the activity significantly decreased with particle size. In addition, the number of electrons exchanged per O_2 molecule increased from a value close to 2–3.4 as the potential was made more negative. They proposed different possible reasons to explain the effect of the particle size, including changes in the stability of surface oxygen species on Au particles of different sizes as a consequence of the different abundance of atoms on edges with respect to those on crystal planes [41], the decrease in number density of {100} surface atoms at these sizes [41], or the stronger adsorption of OH groups on the surface [42].

More recently, Brülle et al. [43] prepared gold nanoparticles with a narrow size distribution deposited on HOPG and single-crystalline boron-doped diamond surfaces using a potentiostatic double-pulse technique. The particle size ranged between 5 and 30 nm on HOPG and between <1 and 15 nm on boron-doped diamond surfaces while keeping the particle density constant. The ORR activity of both samples was studied in 0.1 M H_2SO_4 (Fig. 16.8). Independently of the particle size as well as of the substrate, the specific current densities were always higher than that obtained for a bulk Au electrode. On the other hand, a clear size-dependent ORR activity was observed, increasing the ORR activity with decreasing particle sizes.

This clear size dependence on ORR activity was in agreement with previous observation by Chen and Chen [36]. However, contrarily, Bron [29] reported no size effect for particle sizes in the range between 2.7 and 42 nm supported on carbon black in acidic solutions, whereas Guerin et al. [28] observed that the activity decreased for diameters <3 nm with decreasing particle size. From these previous discussions, it is evident that the effect of Au particle size on the kinetics of O_2 reduction on Au nanoparticles, both in acidic and alkaline media, is a matter of controversy and very different trends can be observed in the literature. In addition, to have a full picture of the situation, it is important to note that theoretical studies predicted an increase in ORR activity with decreasing Au particle size [44]. In our opinion, and in agreement with some of the conclusions reported by Brülle et al. [43],

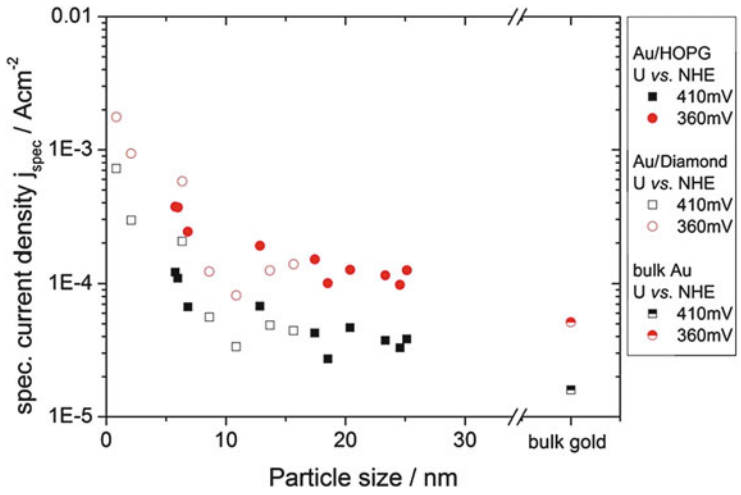

Fig. 16.8 Comparison of the ORR-specific current density for Au/HOPG (*filled symbols*) and Au/diamond (*open symbols*). The current densities versus particle sizes are comparable for the two substrates. The data for an extended gold surface was added as a reference (extracted from [43])

we believe that these discrepancies on particle size trends may be attributed to the strong dependence of the reaction on the surface structure of the nanoparticles. In this regard, it is relevant to point out that in one of the first contributions of our group in this topic [45], we evidenced that gold nanoparticles with a similar particle size (~4 nm) showed different electrocatalytic properties toward ORR as a consequence of their different surface structure and in particular to their different fraction of {100} surface sites. Consequently, as previously demonstrated with Au single-crystal studies, it is of outstanding importance to evaluate the effect of the surface structure of the Au nanoparticles and then correlate it with their electrocatalytic properties. In this context, the correlation between the shape of the nanoparticle and its preferential surface structure is now well established. Thus, as a first approximation, shape will determine which surface structure facets will comprise the surface of the nanoparticle. By controlling their shape, both the reactivity and selectivity of a catalyst can be tailored because the exposed surfaces of the nanoparticle have different surface structures depending on its particular morphology/shape. Very relevant contributions can be already found in the literature about the correlation between the shape/surface structure of different nanoparticles and their electrocatalytic properties [46–55].

16.4 Effect of Shape/Surface Structure

As previously demonstrated from single-crystal studies, Au(100) was the most active catalyst in basic media. Moreover, the overpotential on Au(100) in 0.1 M NaOH is 0.34 V [56] even lower than that on Pt surfaces in 0.1 M $HClO_4$, which is 0.48 V [57]. One of the main strategies to increase the electrocatalytic activity for

ORR has been the preparation of gold nanoparticles containing a high fraction of these {100} surface sites. Therefore, from a crystallographic point of view, the use of cubic Au nanoparticles in which the amount of {100} surface sites is maximized should be a clear goal. Nevertheless, it is very important to note that the critical point determining the electrocatalytic properties is the particular surface structure of the samples and not the shape. Thus, it is of paramount importance to probe the correlation between shape and surface structure on a particular sample. Regarding this issue, one question arises: how can the surface structure of the Au nanoparticles be evaluated and then correlated with their electrocatalytic properties? From transmission electron microscopy (TEM) images, it is relatively easy to determine the preferential shape of the samples. However, the measurement of the different types of sites present on the surface of the nanoparticles by TEM is not simple and requires more specific instrumentation. In this sense, for instance, Gontard et al. [58] showed that spherical-aberration-corrected transmission electron microscopy can be used to provide atomic-resolution information about the local topologies of active sites on commercial nanoparticles with greatly improved sensitivity, as shown in Fig. 16.9. Unfortunately, this kind of analysis is still rather unusual due to the highly sophisticated techniques and time-consuming analyses that are required.

One option could be the analysis of the oxide formation region which, as previously reported by Hamelin et al. [59, 60] with Au single-crystal electrodes, showed different contributions as a function of the specific surface structure. Unfortunately, the inclusion in such high-potential limits would compromise the surface stability of the Au nanoparticles, thus resulting in a surface disordering.

Another possibility to qualitatively measure the amount of the different facets is using surface structure-sensitive reactions which may serve as an indirect technique to estimate the response dependence on the surface geometry of the sample. In this sense, electrodeposition of a monolayer of a given metal on a different substrate at a potential more positive to that of the metal bulk deposition which is known as underpotential deposition (UPD) is generally regarded as a reaction very sensitive to the surface structure of the electrodes [61], since it depends on the specific interaction between the surface atoms of the supporting metal and the depositing atoms of the foreign metal. Lead UPD and its desorption on Au has shown to be a structure-sensitive process [45, 62–65], and the three basal planes give well-defined voltammetric peaks in different potential ranges as shown in Fig. 16.10.

For Au(111) the deposition peak appears at 0.38 V and the dissolution peak at 0.435 V with an overlapping shoulder in the ascending branch. In the case of Au(100), two different contributions appear for both deposition (0.38 and 0.43 V) and dissolution (0.385 and 0.475 V) being those at higher potentials for each process the main peaks. For the Au(110) electrode, the contributions are much broader due to the fact that the process is quite slow. Peaks are centered at 0.50 and 0.56 V for the deposition and dissolution processes. Interestingly, the dissolution peaks for the three basal planes appear at potentials where the other two basal planes have small contributions. Therefore, these contributions at the

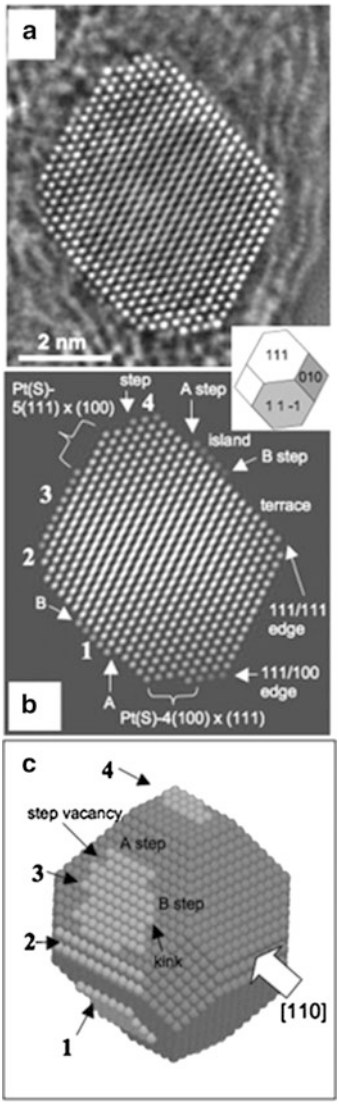

Fig. 16.9 (**a**) Restored phase of a 6 nm Pt particle obtained by applying spherical-aberration correction and through-focus exit wave function restoration to a defocus series of 20 images acquired at 200 kV with the coefficient of spherical aberration, CS, adjusted to −30 μm. (**b**) Best-fitting simulated phase. (**c**) Three-dimensional atomic model used to calculate the best-fitting phase in part (**b**). The *large white arrow* indicates the direction of the electron beam. The *inset* overlapping parts (**a**, **b**) shows the crystallographic details of the particle. In parts (**b**, **c**), 1–4 correspond to the same features on the surface of the particle. The notation Pt(S) − $n(x, y, z)$ × (u, v, w) refers to the microfacets, on which n is the number of atoms in the terrace, (x, y, z) is the Miller index of the terrace, and (u, v, w) is the Miller index of the step (extracted from [58])

aforementioned potentials can be used as indicators of the presence of a particular structure at the surface of a gold electrode.

Surface characterization using Pb UPD of a polycrystalline gold electrode, which is expected to contain all surface sites, shows three main peaks for the dissolution processes at the same potentials that the main dissolution peaks recorded for the three Au basal planes. The only significant difference is that the peak corresponding to the {111} facets is split. Moreover, other small peaks are observed in the voltammetric

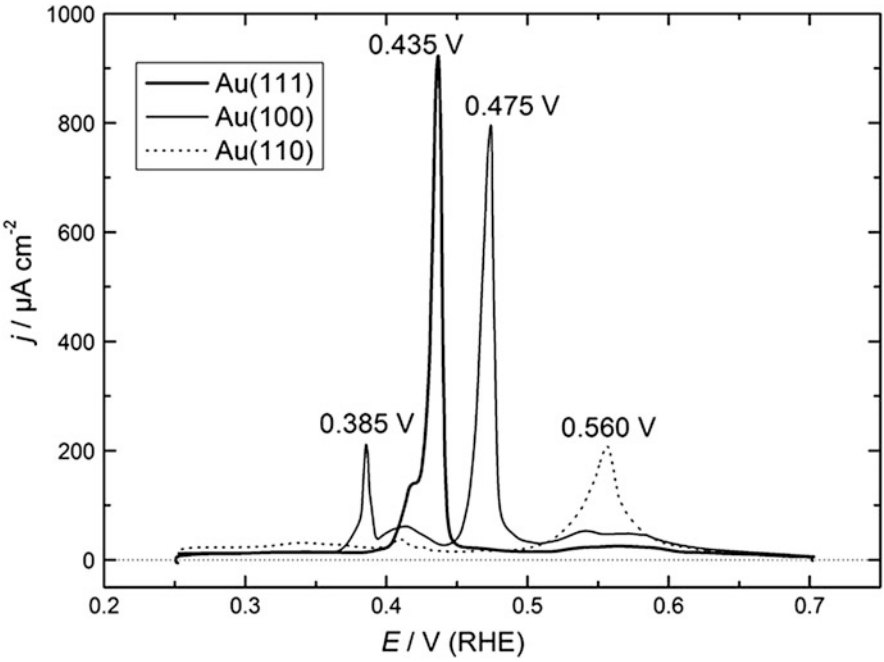

Fig. 16.10 Comparison of the stripping voltammograms for the Pb UPD on the Au(111), Au(100), and Au(110) electrodes in 0.1 M NaOH + 10^{-3} M $Pb(NO_3)_2$. Scan rate = 50 mV s^{-1}

profile, which are ascribed to the dissolution of lead from steps or kinks in the polyoriented surface (especially at potentials below 0.40 V vs. RHE) [45]. The charge of the peaks can be used to qualitatively estimate the relative amount of {100}, {110}, and {111} domains in a polyoriented electrode such as gold nanoparticles. Nevertheless, as it has been observed with stepped surfaces, when domains become smaller, the Pb UPD contributions may take place at different potentials, as observed for Au(775) [45], but the peak shift is small, even for narrow domains, making it positive for nanoparticle electrode characterization, for which domains are expected to be small.

Moreover, Pb UPD can be used to calculate the real area of the electrode from the recorded charge between 0.25 and 0.75 V and assuming a charge density of 420 μC cm^{-2} (measured for a polyoriented surface) [45]. Pb UPD can be also employed to clean the nanoparticles from the organics used during their syntheses by forming an electrochemical PbO_2 film deposited on the gold surface [45, 46, 66–70]. When Pb UPD is performed in basic media (and oxygen reduction is normally studied in these media), the characterization and ORR can be performed in the same medium.

Another interesting option to estimate the fraction of the different surface sites present at the surface of a nanoparticle is the reductive desorption of thiol compounds such as cysteine, mercaptoacetic acid, or cystamine. El-Deab et al., following

previous observations by Porter et al. [71, 72] with polyoriented Au electrodes, used this approach to evaluate the fraction of the surface sites in different types of gold nanostructures [73–75].

One of the first papers in this sense, if not the first, was published by Hernández et al. where gold nanoparticles were synthesized in a water-in-oil microemulsion [45]. In order to modify the surface structure of the Au nanoparticles, iodide and sulfide were added as additives to the water phase of the microemulsion before the chemical reduction with $NaBH_4$. Pb UPD analysis confirmed that those nanoparticles synthesized in the presence of iodide showed a higher ratio of {100} and {111} facets. On the other hand, for those in the presence of sulfide, the two previously mentioned facets were almost missing. Rotating ring-disk experiments for ORR were performed in 0.1 M NaOH with these nanoparticles and the results were compared with additive-free spherical nanoparticles prepared with the same methodology. As expected from single-crystal studies, the gold nanoparticles prepared in the presence of iodide and containing a higher ratio of {100} facets had the highest catalytic activity. As a result, for a surface structure-sensitive reaction as is ORR, a good relationship was obtained between the ratio of {100} facets and the electrocatalytic activity. As previously stated, the evaluation of the amount of the different sites was carried out with Pb UPD and an estimation of the size of the different facets present in the nanoparticles was made by comparing the Pb UPD profile of the nanoparticles with those obtained for the gold single-crystal basal planes.

A similar strategy using additives was used by El-Deab et al. [76] where Au nanoparticles were prepared by adding cysteine or iodide in the electrodeposition bath. Two effects were observed: (1) those nanoparticles prepared in the presence of iodide had a lower particle size (10–40 nm), whereas those prepared with cysteine showed an enhancement of the coalescence of neighboring particles and thus particle sizes of 50–300 nm were observed, and (2) an enrichment of the {100} + {110} facet domains at the expense of the {111} facets was observed in the case of cysteine, while iodide ions enriched the {111} facets of the Au nanoparticles, contrasting with the higher ratio of {111} but also {100} facets shown by Hernández et al. [45], although using different synthesis methods. Therefore, the cysteine-prepared Au nanoparticles exhibited a high catalytic activity for the ORR as previously reported for Au(100) accomplishing a four-electron reduction of oxygen to water at a reasonably low cathodic overpotential in O_2-saturated 0.5 M KOH. These findings were more deeply studied by the same group in different publications [74, 77–79]. In one of these papers, the effect of the support was also evaluated [79]. Interestingly, when HOPG was used, an electrooxidative pretreatment of the support led to more active cysteine-prepared Au nanoparticles in comparison with untreated HOPG. On the other hand, no improvement was observed in the case of using iodide as additive.

Another strategy was to synthesize nanoparticles with shapes that would have a preferential surface structure. Concerning this idea, oxygen reduction reaction on some shape-controlled gold nanoparticles was reviewed in 2009 [46]. In this sense Hernández et al. studied the ORR with gold nanorods [67]. Their surface structure

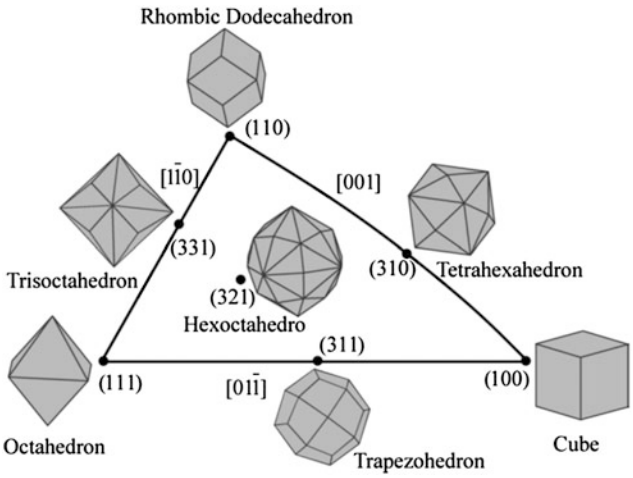

Fig. 16.11 Unit stereographic triangle of polyhedral nanocrystals bounded by different crystal planes (extracted from [83])

was analyzed with Pb UPD, revealing that their nanorods were composed by {111} and {110} domains, while {100} domains were practically absent. Hydrogen peroxide was the final product in the whole potential range confirming the absence of {100} sites as obtained from the Pb UPD analysis. This conclusion was in agreement with HRTEM images which indicated that the side faces of the nanorods were {110} faces [80] and with selective area electron diffraction (SAED) experiments, which indicated that the nanorods were capped at both ends by five {111} faces [81]. Nevertheless, Gao et al. observed a higher activity of Au nanorods in comparison with spherical nanoparticles but their synthesis conditions were different [82]. In this case the authors used an electrodeposition method in the presence of cysteine, which as mentioned before produced an enrichment of the {100} + {110} facet domains at the expense of the {111} facets [76]. For the nanorods the authors explained the behavior of a continuous unidirectional growth of the crystal along the {111} orientation, leading to a pin-like morphology of the crystals.

In analogy with the stereographic triangle where the three basal planes are located at the vertices, an intrinsic triangle can be made which coordinates the crystal surface index and the shape of fcc metal nanocrystals as shown in Fig. 16.11 [83, 84]. The three vertices represent the coordinates of polyhedral nanocrystals bounded by basal facets, i.e., cube covered by {100}, octahedron by {111}, and rhombic dodecahedron by {110} faces.

Nevertheless, as previously stated, it is important to recall that the main issue is the final arrangement of the atoms at the surface, which may not be that expected from the nanoparticle shape. This fact highlights the importance of characterization tools such as Pb UPD. Going back to the analogy with the stereographic triangle, if from single-crystal knowledge it is known that Au(100) is the most active catalyst

in alkaline medium, it seems interesting to study the ORR with gold nanocubes. Hernández et al. prepared this type of gold nanoparticles for this purpose [69]. Deliberately, the authors synthesized large cubic Au nanoparticles (average size 40 nm) using a seed-mediated method in the presence of cetyltrimethylammonium bromide. SAED patterns confirmed that the cubic nanoparticles were single crystals. Although lead UPD confirmed the presence of a large amount of {100} domains, the majority of the surface sites had a {111} or {110} symmetry, suggesting that surface faceting or ripening had taken place. Nevertheless, due to the large amount of {100} sites, this type of nanoparticles showed a very high catalytic activity for the four-electron oxygen reduction paths in alkaline medium. As a result, water was obtained as the final product of the reaction in the whole potential range, except in the lower potential range where hydrogen peroxide was obtained, in a similar way as reported for Au(100). Moreover, the authors studied the stability of the surface of the cubic nanoparticles during the electrocatalytic experiments performing Pb UPD experiments after the ORR. Although the reactivity was maintained, the amount of {100} domains decreased, concluding that the transport-controlled reaction of interest is less sensitive to the surface order.

The electrocatalytic activity of the different samples can be addressed using the scanning electrochemical microscopy (SECM). Thus several samples can be probed simultaneously, allowing a direct comparison. The activity for the ORR of different shape-controlled gold nanoparticles and nanorods was studied by Sánchez-Sánchez et al. [70]. The different shaped nanoparticles were characterized by TEM and Pb UPD, providing information on the shape and surface structure of the different nanoparticles (spherical and cubic) and short nanorods. Cubic gold nanoparticles were the most active toward ORR in alkaline medium followed by the spherical nanoparticles and being the short nanorods the least active, as shown in Fig. 16.12. These results are expected taking into account single-crystal results and from the fact that a nanocube is ideally enclosed by six {100} faces. These results were also in agreement with previous works from the same research group [45, 67, 69].

Nanopyramidal, nanorod-like, and spherical gold nanostructures were also used to study the ORR in 0.5 M KOH [85]. They were synthesized on polycrystalline gold substrates through electrochemical overpotential deposition by manipulating the deposited potentials and concentrations of $HAuCl_4$. X-ray diffraction and electrochemical experiments showed that the pyramidal structures were dominated by {111} facets, and therefore due to the lowest amount of {100} sites, the activity toward ORR was the lowest. The reduction peak current increased and the peak potential shifted positively in the following order: nanopyramids $<$ nanorods $<$ nanospheres.

El-Deab studied the influence of the electrodeposition time on the crystallographic orientation of Au nanoparticles electrodeposited on glassy carbon prepared by potential step electrolysis and on their electrocatalytic properties toward ORR in alkaline medium (0.5 M KOH) [73]. He observed that particles prepared in short time (5–60 s) had smaller size (10–50 nm) and showed a higher particle density (number of particles per unit area), as revealed by SEM images, than those prepared

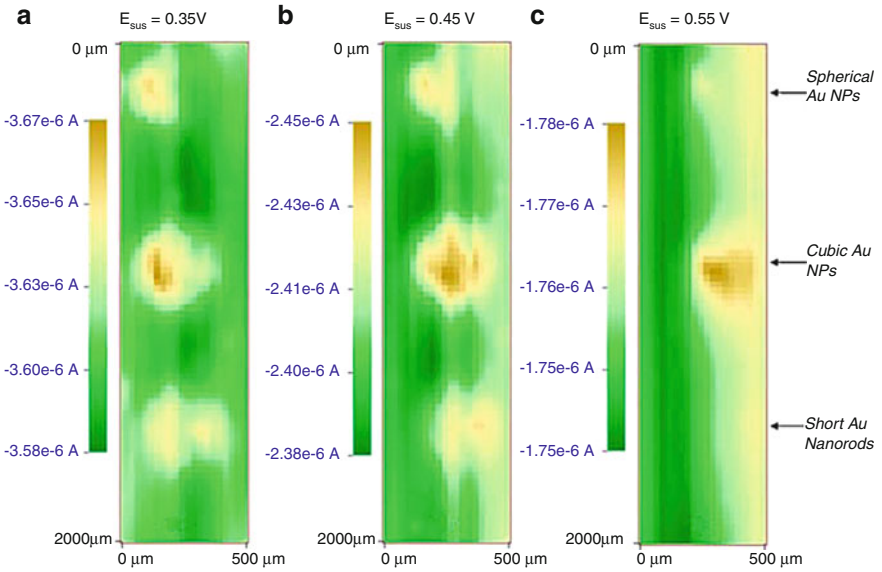

Fig. 16.12 SECM TG-SC images displaying the substrate current for ORR of an array composed by 3 different types of shape-controlled gold particles supported on a glassy carbon plate. Substrate potential held constant at (**a**) 0.35 V, (**b**) 0.45 V, and (**c**) 0.55 V versus RHE in an oxygen-free 0.1 M NaOH solution. Tip-substrate distance = 25 µm. Oxygen flux generated at the tip at a constant current of 150 nA. Scan rate = 125 µm s^{-1} (extracted from [70])

by longer electrolysis time. On the other hand, Au deposits prepared for times higher than 60 s were larger (>100 nm). SEM, XRD, and electron backscatter diffraction (EBSD) techniques were used to characterize both the size and preferential facet orientation of the nanoparticles. Interestingly from the EBSD patterns, the author estimated the fraction for the {100} {110}, and {111} orientations corresponding to the Au samples being the total fraction of a specific facet, the percentage of a specific orientation relative to the total area of the analyzed region of the surface [86]. From EBSD analysis the author found that increasing the deposition time resulted in an increase in the total fraction of {100} and {110} facets, while for short deposition times the deposit was rich in {111} facets. ORR was studied with gold nanoparticles prepared after 60, 300, and 900 s and showed to be influenced by the surface structure as shown in Fig. 16.13. The sample enriched with {111} domains (60 s) had a much lower activity than those containing a lower fraction of {111} surface domains (300 and 900 s), being the peak current density about 1.7 times higher than those prepared after 60 s. This difference was ascribed to the increase of the number of exchanged electrons as a consequence of their polycrystalline surface structure instead of a {111} enriched. In fact the behavior was very similar for the polycrystalline bulk Au electrode and those nanoparticles prepared after longtime deposits. In addition, a possible particle size effect was ruled out because the diffusion layer thickness ($\delta \approx 0.021$ cm) was much larger than the average distance between Au nanoparticles (≈50–200 nm).

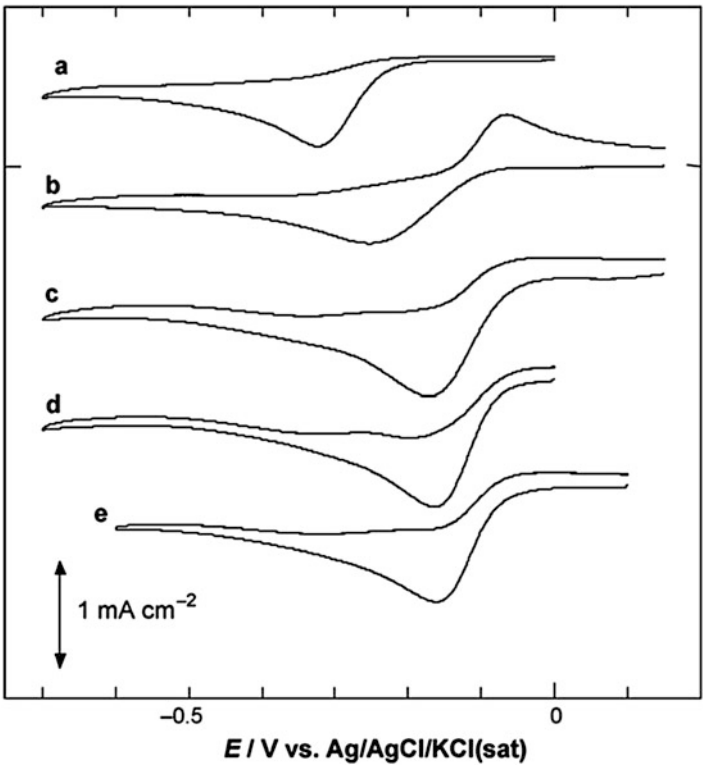

Fig. 16.13 CVs measured at 100 mV s^{-1} for the oxygen reduction at (a) bare GC, (b) 60 s nano-Au/GC, (c) 300 s nano-Au/GC, (d) 900 s nano-Au/GC, and (e) bare polycrystalline Au electrodes in O_2-saturated 0.5 M KOH (extracted from [73])

Several strategies have been used to maximize the electrocatalytic activity of the gold nanoparticles by tailoring the shape. Xu et al. [87] studied the ORR with indium tin oxide (ITO)-supported dendritic gold nanostructures prepared with a "green" templateless, surfactantless, simple electrochemical route. The samples were characterized by scanning electron microscopy (SEM), TEM, energy-dispersive X-ray spectroscopy (EDX), X-ray diffraction (XRD), and X-ray photoelectron spectroscopy (XPS). The dendritic gold nanostructures showed an improved behavior toward ORR in comparison to a bulk gold electrode in neutral O_2-saturated KCl solution as the peak position shifted about 0.2 V positively and the peak current increased significantly. In the voltammogram for the oxygen reduction with the dendritic gold nanostructure, two different reduction peaks were observed, the first one corresponding to oxygen reduction to H_2O_2 and the second peak corresponding to the reduction of H_2O_2 to H_2O, which was confirmed by adding H_2O_2 to the solution. Similar results were obtained by Jena and Raj [88], who synthesized branched flowerlike gold nanocrystals using *N*-2-hydroxyethylpiperazine-*N*-2-ethanesulphonic acid as reducing/stabilizing agent. These nanomaterials were self-assembled on a

solgel-derived silicate network, which was preassembled on a polycrystalline Au electrode, and they retained their morphology on the silicate network. Their electrocatalytic activity toward ORR was higher than that of citrate-stabilized Au nanoparticles, being the reduction of oxygen to hydrogen peroxide and its oxidation to water in neutral pH (phosphate buffer) observed at more positive potentials. The same authors also studied this reaction using triangular gold nanoprisms (70–110 nm) and nanoperiwinkles (150–230 nm), also self-assembled on a three-dimensional silicate network [89]. The samples were prepared using 5-hydroxytryptamine as a reducing/stabilizing agent at room temperature. Although the X-ray diffraction profiles of both samples revealed that they were composed mainly of a Au(111) lattice plane, both structures showed higher electrocatalytic activity than spherical gold nanoparticles.

Kuai et al. prepared icosahedral Au nanoparticles through a facile, one-pot, seedless, water-based method and studied ORR with them [90]. The growth mechanism indicated that the icosahedral nanoparticles were formed from multiple-twinned seeds and PVP was used both as reducing agent and surfactant. In spite of the fact that icosahedra are enclosed by {111} facets, the authors found higher electrocatalytic activities than sphere-like nanoparticles for ORR in alkaline medium. In fact, the reduction peak for oxygen reduction was positively shifted 0.05 V for icosahedra and also their peak current was 1.6-fold higher than that of spherical nanoparticles. Moreover, the gold icosahedra displayed even lower overpotential than a commercial Pt/C electrocatalyst.

The electrocatalytic activity of gold nanoplates toward ORR in 0.1 M NaOH was also evaluated. Seo et al. prepared this type of nanomaterials by reducing $KAu(CN)_2$ in a Na_2CO_3 solution at a constant potential [91]. The prepared nanoplates were rich in {110} and {100} domains (studied by Pb UPD) and exhibited higher electrocatalytic activity than bare gold for ORR. Both the peak potential for oxygen reduction shifted positively (about 70–80 mV) and the current density increased (about three times) for the nanoplates in comparison with bare Au. In addition, to get information about the reduction mechanism, the authors also performed RDE experiments and found that the number of electrons associated with the oxygen reduction was 4 for the nanoplate electrode, while on bare Au was 2, thus indicating the effective four-electron reduction of oxygen to water in alkaline medium for the Au nanoplates.

Das and Raj observed also an enhancement in the electrocatalytic activity toward ORR with penta-twined Au nanostructures (average size 52 nm) in neutral medium [92]. These nanomaterials were prepared using piperazine derivatives in the absence of seeds or surfactants and were characterized by TEM (average size 52 nm) and X-ray diffraction, which revealed the existence of face-centered cubic nanocrystalline Au. The penta-twined nanostructures were reported to catalyze the reduction of oxygen in neutral solution to water through the formation of hydrogen peroxide. Two well-defined peaks corresponding to the reduction of oxygen to hydrogen peroxide and the further reduction of electrogenerated hydrogen peroxide to water were obtained. A significant increase in the peak current (1.6 times) and a decrease in the overpotential for the ORR were observed in comparison with spherical nanoparticles. In fact, the reduction peak potential for the spherical nanoparticles

was considerably more negative (~120 mV) than that of the penta-twined nanoparticles. Moreover, the onset potential for the penta-twined nanoparticles was 80–90 mV more positive than for the spherical nanoparticles.

Plowman et al. reported a very interesting contribution determining what the surface active sites responsible of the activity of different nanostructured gold electrodes are [93]. In this work they studied anisotropic Au, well-dispersed hierarchical Au, and continuous porous honeycomb Au structures. The analysis was carried out under acidic and alkaline conditions using electrochemical techniques such as cyclic voltammetry and a large-amplitude Fourier transformed alternating current (FT-ac) method which can effectively discriminate between capacitive and faradaic processes occurring at an electrode surface. Interestingly, it was observed that the response of these electrodes is similar to that observed for activated gold electrodes whose surfaces have been treated by cathodic polarization in the hydrogen evolution region. According to the authors, this activation results in the disruption of the outer layers of the metal to create an active surface. These active sites, which are believed to consist of low-coordinated active gold sites, or clusters of atoms, are more readily oxidized than the bulk Au electrodes. This more facile oxidation of active gold results in significant electrochemical responses recorded in the double-layer region. In particular, they reported the reduction of oxygen both in acid and alkaline media with the porous honeycomb Au structures. The results obtained indicated that the ORR commences at potentials where the surface active sites responses were observed.

Finally, some electrochemical treatments have been also used to change the surface structure of the gold nanoparticles, so that higher activity for the ORR is obtained. Shim et al. also studied the effect of an electrochemical pretreatment in a 0.05 M phosphate buffer solution (pH ~7.4) on bulk Au and Au nanoparticles (~10 nm diameter) toward the ORR [94]. Both samples were electrochemically pretreated by repetitive potential cycling between −0.2 and 1 V (vs. SCE) for 200 cycles at a scan rate of 50 mV s^{-1}. The RDE voltammetric experiments showed that after the pretreatment, the ORR activity was enhanced in both samples. The number of electrons for both pretreated samples became close to 4, the onset potential became more positive, and the currents became higher. Moreover, nanoparticles' performance was better than that of bulk Au. The authors attributed the enhanced catalytic activity to the formation of a thick Au oxide layer, which was corroborated with a thermally pretreated Au microwire electrode. Moreover, the authors claimed that the Au oxide layer was able to adsorb O_2 more favorably than the initial Au surface. In addition, the pretreated bulk and nanoparticles also showed higher activity toward the oxidation of hydrogen peroxide than the corresponding untreated ones.

Chen et al. [95], very recently, prepared Au thin-film electrodes made by electroless deposition for in situ electrochemical attenuated total-reflection surface-enhanced infrared adsorption spectroscopy (ATR-SEIRAS) which consisted of ~46 nm Au nanoparticles deposited on a Si infrared window. Very interestingly, they observed that a square-wave treatment of the Au film led to a much enhanced ORR activity (O_2-saturated 0.1 M $HClO_4$) as a consequence of the surface reconstruction of the nanoparticle film. Thus, whereas the ORR activity of the initial Au

film electrode was similar to that obtained with a polycrystalline Au in acid solution, after the square-wave potential treatment, a remarkable shift to positive potential of about 0.14 V on the ORR half-wave potential was observed. In addition, the Tafel slope changed from 119 to 90 mV, indicating a modification in the rate-determining step. From SEM images, they observed that the square-wave treatment caused a significant surface reconstruction by "melting" the Au nanoparticles, thus leading to a more continuous Au electrode surface. However, from the analysis of the voltammetric curves in the Au oxide region, they observed that the {100} surface sites remained almost intact or even increased slightly in this reconstructed surface, whereas the characteristic signal of the {111} and {110} sites decreased. Nevertheless, the enhanced ORR activity was not attributed to the {100} orientation of the reconstructed film but to the formation of a new type of surface sites whose oxide reduction peak was observed at 0.4 V versus Ag/AgCl once the upper potential limit was more positive than 1 V. The experimental evidences indicated that this new type of surface sites was responsible of the ORR activity enhancement, and they suggested that these new sites could stabilize better the adsorbed ORR intermediates, thus facilitating the subsequent reaction step(s). More work is still needed to understand the nature and electrochemical properties of this type of surface sites.

16.5 Conclusions

The results presented in this chapter clearly indicate that the reactivity of gold for the ORR is mainly controlled by the surface structure. In alkaline medium, the Au(100) electrode shows a high activity transferring four electrons at high potentials, whereas a much lower activity with the transfer of only two electrons is observed for the Au(111) and Au(110) electrodes. The strong surface structure sensitivity results in a significant effect of the shape of the nanoparticles in the reactivity for this reaction. Thus, for nanoparticles with similar size, the reactivity depends mainly on the fraction of {100} domains on the surface.

Acknowledgments This work has been financially supported by the MICINN (Spain) (project CTQ2010-16271) and Generalitat Valenciana (project PROMETEO/2009/045, FEDER).

References

1. Adzic RR (1998) Recent advances in the kinetics of oxygen reduction. In: Lipkowski J, Ross PN (eds) Electrocatalysis. Wiley, New York, pp 197–242
2. Anastasijević NA, Vesović V, Adžić RR (1987) Determination of the kinetic parameters of the oxygen reduction reaction using the rotating ring-disk electrode: Part I. Theory. J Electroanal Chem 229(1–2):305–316
3. Anastasijević NA, Vesović V, Adžić RR (1987) Determination of the kinetic parameters of the oxygen reduction reaction using the rotating ring-disk electrode: Part II. Applications. J Electroanal Chem 229(1–2):317–325

4. Alvarez-Rizatti M, Jüttner K (1983) Electrocatalysis of oxygen reduction by UPD of lead on gold single-crystal surfaces. J Electroanal Chem 144(1–2):351–363
5. Sayed SM, Jüttner K (1983) Electrocatalysis of oxygen and hydrogen peroxide reduction by UPD of bismuth on poly- and mono-crystalline gold electrodes in acid solutions. Electrochim Acta 28(11):1635–1641
6. Adžić RR, Marković NM (1982) Structural effects in electrocatalysis: oxygen and hydrogen peroxide reduction on single crystal gold electrodes and the effects of lead ad-atoms. J Electroanal Chem 138(2):443–447
7. Markovic NM, Adzic RR, Vesovic VB (1984) Structural effects in electrocatalysis Oxygen reduction on the gold single crystal electrodes with (110) and (111) orientations. J Electroanal Chem 165:121–133
8. Adžić RR, Marković NM, Vesović VB (1984) Structural effects in electrocatalysis. Oxygen reduction on the Au (100) single crystal electrode. J Electroanal Chem 165(1–2):105–120
9. Štrbac S, Adžić RR (1992) Oscillatory phenomena in oxygen and hydrogen peroxide reduction on the Au(100) electrode surface in alkaline solutions. J Electroanal Chem 337(1–2):355–364
10. Štrbac S, Anastasijević NA, Adžić RR (1992) Oxygen reduction on Au (100) and vicinal Au (910) and Au (11, 1, 1) faces in alkaline solution: a rotating disc-ring study. J Electroanal Chem 323(1–2):179–195
11. Polewska W, Vitus CM, Ocko BM, Adzic RR (1994) Direct observation of the Au(100) reconstruction during the course of O2 reduction in alkaline solution. J Electroanal Chem 364(1–2):265–269
12. Štrbac S, Anastasijević NA, Adžić RR (1994) Oxygen reduction on Au(111) and vicinal Au (332) faces: a rotating disc and disc-ring study. Electrochim Acta 39(7):983–990
13. Prieto A, Hernández J, Herrero E, Feliu JM (2003) The role of anions in oxygen reduction in neutral and basic media on gold single-crystal electrodes. J Solid State Electrochem 7(9):599–606
14. Koper MTM (1998) Non-linear phenomena in electrochemical systems. J Chem Soc Faraday Trans 94(10):1369–1378
15. Štrbac S, Adžić RR (1996) The influence of OH- chemisorption on the catalytic properties of gold single crystal surfaces for oxygen reduction in alkaline solutions. J Electroanal Chem 403 (1–2):169–181
16. Anastasijević NA, Štrbac S, Adžić RR (1988) Oxygen reduction on the Au (311) electrode surface in alkaline electrolyte. J Electroanal Chem 240(1–2):239–252
17. Strbac S, Adzic RR (1996) The influence of pH on reaction pathways for O-2 reduction on the Au(1 00) face. Electrochim Acta 41(18):2903–2908
18. Wu B-l, Lei H-w, Cha C-s, Chen Y-y (1994) Investigation of the intermediates of the O_2 reduction reaction on Au electrodes in alkaline solution. J Electroanal Chem 377 (1–2):227–230
19. Vassilev P, Koper MTM (2007) Electrochemical reduction of oxygen on gold surfaces: a density functional theory study of intermediates and reaction paths. J Phys Chem C 111(6):2607–2613
20. Blizanac BB, Lucas CA, Gallagher ME, Arenz M, Ross PN, Marković NM (2003) Anion adsorption, CO oxidation, and oxygen reduction reaction on a Au(100) surface: the pH effect. J Phys Chem B 108(2):625–634
21. Sarapuu A, Tammeveski K, Tenno TT, Sammelselg V, Kontturi K, Schiffrin DJ (2001) Electrochemical reduction of oxygen on thin-film Au electrodes in acid solution. Electrochem Commun 3(8):446–450
22. El-Deab MS, Ohsaka T (2002) An extraordinary electrocatalytic reduction of oxygen on gold nanoparticles-electrodeposited gold electrodes. Electrochem Commun 4(4):288–292
23. Zhang Y, Asahina S, Yoshihara S, Shirakashi T (2003) Oxygen reduction on Au nanoparticle deposited boron-doped diamond films. Electrochim Acta 48(6):741–747
24. El-Deab MS, Ohsaka T (2002) Hydrodynamic voltammetric studies of the oxygen reduction at gold nanoparticles-electrodeposited gold electrodes. Electrochim Acta 47(26):4255–4261

25. El-Deab MS, Ohsaka T (2003) Electrocatalysis by nanoparticles: oxygen reduction on gold nanoparticles-electrodeposited platinum electrodes. J Electroanal Chem 553(suppl):107–115
26. El-Deab MS, Okajima T, Ohsaka T (2003) Electrochemical reduction of oxygen on gold nanoparticle-electrodeposited glassy carbon electrodes. J Electrochem Soc 150(7): A851–A857
27. Yagi I, Ishida T, Uosaki K (2004) Electrocatalytic reduction of oxygen to water at Au nanoclusters vacuum-evaporated on boron-doped diamond in acidic solution. Electrochem Commun 6(8):773–779
28. Guerin S, Hayden BE, Pletcher D, Rendall ME, Suchsland JP (2006) A combinatorial approach to the study of particle size effects on supported electrocatalysts: oxygen reduction on gold. J Comb Chem 8(5):679–686
29. Bron M (2008) Carbon black supported gold nanoparticles for oxygen electroreduction in acidic electrolyte solution. J Electroanal Chem 624(1–2):64–68
30. Sarapuu A, Nurmik M, Mandar H, Rosental A, Laaksonen T, Kontturi K, Schiffrin DJ, Tammeveski K (2008) Electrochemical reduction of oxygen on nanostructured gold electrodes. J Electroanal Chem 612(1):78–86
31. Maruyama J, Inaba M, Ogumi Z (1999) Effect of fluorinated alcohol on the kinetics of cathodic oxygen reduction at gold electrodes. Electrochim Acta 45(3):415–422
32. Maruyama J, Inaba M, Morita T, Ogumi Z (2001) Effects of the molecular structure of fluorinated additives on the kinetics of cathodic oxygen reduction. J Electroanal Chem 504(2):208–216
33. Tang W, Lin H, Kleiman-Shwarsctein A, Stucky GD, McFarland EW (2008) Size-dependent activity of gold nanoparticles for oxygen electroreduction in alkaline electrolyte. J Phys Chem C 112(28):10515–10519
34. Inasaki T, Kobayashi S (2009) Particle size effects of gold on the kinetics of the oxygen reduction at chemically prepared Au/C catalysts. Electrochim Acta 54(21):4893–4897
35. Erikson H, Jürmann G, Sarapuu A, Potter RJ, Tammeveski K (2009) Electroreduction of oxygen on carbon-supported gold catalysts. Electrochim Acta 54(28):7483–7489
36. Chen W, Chen S (2009) Oxygen electroreduction catalyzed by gold nanoclusters: strong core size effects. Angew Chem Int Ed 48(24):4386–4389
37. Li Y, Cox JT, Zhang B (2010) Electrochemical responses and electrocatalysis at single Au nanoparticles. J Am Chem Soc 132(9):3047–3054
38. Lee Y, Loew A, Sun S (2009) Surface- and structure-dependent catalytic activity of Au nanoparticles for oxygen reduction reaction. Chem Mater 22(3):755–761
39. Alexeyeva N, Matisen L, Saar A, Laaksonen P, Kontturi K, Tammeveski K (2010) Kinetics of oxygen reduction on gold nanoparticle/multi-walled carbon nanotube hybrid electrodes in acid media. J Electroanal Chem 642(1):6–12
40. Jirkovsky JS, Halasa M, Schiffrin DJ (2010) Kinetics of electrocatalytic reduction of oxygen and hydrogen peroxide on dispersed gold nanoparticles. Phys Chem Chem Phys 12(28):8042–8052
41. Kinoshita K (1990) Particle size effects for oxygen reduction on highly dispersed platinum in acid electrolytes. J Electrochem Soc 137(3):845–848
42. Mayrhofer KJJ, Blizanac BB, Arenz M, Stamenkovic VR, Ross PN, Markovic NM (2005) The impact of geometric and surface electronic properties of Pt-catalysts on the particle size effect in electrocatalysis. J Phys Chem B 109(30):14433–14440
43. Brülle T, Ju W, Niedermayr P, Denisenko A, Paschos O, Schneider O, Stimming U (2011) Size-dependent electrocatalytic activity of gold nanoparticles on HOPG and highly boron-doped diamond surfaces. Molecules 16(12):10059–10077
44. Greeley J, Rossmeisl J, Hellman A, Nørskov JK (2007) Theoretical trends in particle size effects for the oxygen reduction reaction. Z Phys Chem 221(9–10):1209–1220
45. Hernández J, Solla-Gullón J, Herrero E (2004) Gold nanoparticles synthesized in a water-in-oil microemulsion: electrochemical characterization and effect of the surface structure on the oxygen reduction reaction. J Electroanal Chem 574(1):185–196

46. Hernández J, Solla-Gullón J, Herrero E, Feliu JM, Aldaz A (2009) In situ surface characterization and oxygen reduction reaction on shape-controlled gold nanoparticles. J Nanosci Nanotechnol 9(4):2256–2273
47. Solla-Gullon J, Vidal-Iglesias FJ, Feliu JM (2011) Shape dependent electrocatalysis. Annu Rep Prog Chem C Phys Chem 107:263–297
48. Koper MTM (2011) Structure sensitivity and nanoscale effects in electrocatalysis. Nanoscale 3(5):2054–2073
49. Cheng Q, Jiang Y-X, Tian N, Zhou Z-Y, Sun S-G (2010) Electrocatalytic reduction of nitric oxide on Pt nanocrystals of different shape in sulfuric acid solutions. Electrochim Acta 55(27):8273–8279
50. Vidal-Iglesias FJ, Solla-Gullón J, Rodríguez P, Herrero E, Montiel V, Feliu JM, Aldaz A (2004) Shape-dependent electrocatalysis: ammonia oxidation on platinum nanoparticles with preferential (100) surfaces. Electrochem Commun 6(10):1080–1084
51. Solla-Gullón J, Vidal-Iglesias FJ, Rodríguez P, Herrero E, Feliu JM, Aldaz A (2006) Shape-dependent electrocatalysis: CO monolayer oxidation at platinum nanoparticles. In: Brisard GM, Adzic R, Birss V, Vieckowski A (eds) Proceedings – Electrochemical Society 2005–11 (Electrocatalysis). The Electrochemical Society, Pennington, NJ, pp 1–11
52. Solla-Gullón J, Vidal-Iglesias FJ, Herrero E, Feliu JM, Aldaz A (2006) CO monolayer oxidation on semi-spherical and preferentially oriented (100) and (111) platinum nanoparticles. Electrochem Commun 8(1):189–194
53. Solla-Gullón J, Vidal-Iglesias FJ, López-Cudero A, Garnier E, Feliu JM, Aldaz A (2008) Shape-dependent electrocatalysis: methanol and formic acid electrooxidation on preferentially oriented Pt nanoparticles. Phys Chem Chem Phys 10(25):3689–3698
54. Sanchez-Sanchez CM, Solla-Gullon J, Vidal-Iglesias FJ, Aldaz A, Montiel V, Herrero E (2010) Imaging structure sensitive catalysis on different shape-controlled platinum nanoparticles. J Am Chem Soc 132(16):5622–5624
55. Erikson H, Sarapuu A, Tammeveski K, Solla-Gullón J, Feliu JM (2011) Enhanced electrocatalytic activity of cubic Pd nanoparticles towards the oxygen reduction reaction in acid media. Electrochem Commun 13(7):734–737
56. Adžić RR, Strbac S, Anastasijević N (1989) Electrocatalysis of oxygen on single crystal gold electrodes. Mater Chem Phys 22(3–4):349–375
57. Marković NM, Adžić RR, Cahan BD, Yeager EB (1994) Structural effects in electrocatalysis: oxygen reduction on platinum low index single-crystal surfaces in perchloric acid solutions. J Electroanal Chem 377(1–2):249–259
58. Gontard LC, Chang LY, Hetherington CJD, Kirkland AI, Ozkaya D, Dunin-Borkowski RE (2007) Aberration-corrected imaging of active sites on industrial catalyst nanoparticles. Angew Chem Int Ed 46(20):3683–3685
59. Hamelin A (1996) Cyclic voltammetry at gold single-crystal surfaces. 2. Behaviour of high-index faces. J Electroanal Chem 407(1–2):13–21
60. Hamelin A (1996) Cyclic voltammetry at gold single-crystal surfaces. 1. Behaviour at low-index faces. J Electroanal Chem 407(1–2):1–11
61. Herrero E, Buller LJ, Abruna HD (2001) Underpotential deposition at single crystal surfaces of Au, Pt, Ag and other materials. Chem Rev 101(7):1897–1930
62. Hamelin A (1979) Lead adsorption on gold single crystal stepped surfaces. J Electroanal Chem 101(2):285–290
63. Hamelin A, Katayama A (1981) Lead underpotential deposition on gold single-crystal surfaces: the (100) face and its vicinal faces. J Electroanal Chem 117(2):221–232
64. Hamelin A (1984) Underpotential deposition of lead on single crystal faces of gold. Part I. The influence of crystallographic orientation of the substrate. J Electroanal Chem 165(1–2):167–180
65. Hamelin A, Lipkowski J (1984) Underpotential deposition of lead on gold single crystal faces. Part II. General discussion. J Electroanal Chem 171(1–2):317–330

66. Hernández J, Herrero E, Solla-Gullón J, Vidal-Iglesias FJ, Feliu JM, Aldaz A (2006) Shape-dependent electrocatalysis: oxygen reduction on gold nanoparticles. In: Brisard GM, Adzic R, Birss V, Vieckowski A (eds) Proceedings – Electrochemical Society 2005–11 (Electrocatalysis). The Electrochemical Society, Pennington, NJ, pp 200–212
67. Hernández J, Solla-Gullón J, Herrero E, Aldaz A, Feliu JM (2005) Characterization of the surface structure of gold nanoparticles and nanorods using structure sensitive reactions. J Phys Chem B 109(26):12651–12654
68. Hernández J, Solla-Gullón J, Herrero E, Aldaz A, Feliu JM (2006) Methanol oxidation on gold nanoparticles in alkaline media: unusual electrocatalytic activity. Electrochim Acta 52(4):1662–1669
69. Hernández J, Solla-Gullón J, Herrero E, Aldaz A, Feliu JM (2007) Electrochemistry of shape-controlled catalysts: oxygen reduction reaction on cubic gold nanoparticles. J Phys Chem C 111(38):14078–14083
70. Sanchez-Sanchez CM, Vidal-Iglesias FJ, Solla-Gullon J, Montiel V, Aldaz A, Feliu JM, Herrero E (2010) Scanning electrochemical microscopy for studying electrocatalysis on shape-controlled gold nanoparticles and nanorods. Electrochim Acta 55(27):8252–8257
71. Walczak MM, Alves CA, Lamp BD, Porter MD (1995) Electrochemical and X-ray photoelectron spectroscopic evidence for differences in the binding sites of alkanethiolate monolayers chemisorbed at gold. J Electroanal Chem 396(1–2):103–114
72. Zhong CJ, Zak J, Porter MD (1997) Voltammetric reductive desorption characteristics of alkanethiolate monolayers at single crystal Au(111) and (110) electrode surfaces. J Electroanal Chem 421(1–2):9–13
73. El-Deab MS (2009) On the preferential crystallographic orientation of Au nanoparticles: effect of electrodeposition time. Electrochim Acta 54(14):3720–3725
74. El-Deab MS, Sotomura T, Ohsaka T (2005) Size and crystallographic orientation controls of gold nanoparticles electrodeposited on GC electrodes. J Electrochem Soc 152(1):C1–C6
75. El-Deab MS, Arihara K, Ohsaka T (2004) Fabrication of Au(111)-like polycrystalline gold electrodes and their applications to oxygen reduction. J Electrochem Soc 151(6):E213–E218
76. El-Deab MS, Sotomura T, Ohsaka T (2005) Oxygen reduction at electrochemically deposited crystallographically oriented Au(1 0 0)-like gold nanoparticles. Electrochem Commun 7(1):29–34
77. El-Deab MS, Sotomura T, Ohsaka T (2005) Morphological selection of gold nanoparticles electrodeposited on various substrates. J Electrochem Soc 152(11):C730–C737
78. Gao F, El-Deab MS, Okajima T, Ohsaka T (2005) Electrochemical preparation of a Au crystal with peculiar morphology and unique growth orientation and its catalysis for oxygen reduction. J Electrochem Soc 152(6):A1226–A1232
79. El-Deab MS, Sotomura T, Ohsaka T (2006) Oxygen reduction at Au nanoparticles electrodeposited on different carbon substrates. Electrochim Acta 52(4):1792–1798
80. Gai PL, Harmer MA (2002) Surface atomic defect structures and growth of gold nanorods. Nano Lett 2(7):771–774
81. Johnson CJ, Dujardin E, Davis SA, Murphy CJ, Mann S (2002) Growth and form of gold nanorods prepared by seed-mediated, surfactant-directed synthesis. J Mater Chem 12(6):1765–1770
82. Gao F, El-Deab MS, Ohsaka T (2005) Electrodeposition of gold nanorods with a unidirectional crystal growth and lower Au(111) facets area. Indian J Chem A 44(5):932–937
83. Zhou Z-Y, Tian N, Huang Z-Z, Chen D-J, Sun S-G (2009) Nanoparticle catalysts with high energy surfaces and enhanced activity synthesized by electrochemical method. Faraday Discuss 140:81–92
84. Tian N, Zhou ZY, Sun SG (2008) Platinum metal catalysts of high-index surfaces: from single-crystal planes to electrochemically shape-controlled nanoparticles. J Phys Chem C 112(50):19801–19817
85. Tian Y, Liu H, Zhao G, Tatsuma T (2006) Shape-controlled electrodeposition of gold nanostructures. J Phys Chem B 110(46):23478–23481

86. Koblischka-Veneva A, Koblischka MR (2008) Analysis of twin boundaries using the electron backscatter diffraction (EBSD) technique. Mater Sci Eng B Solid State Mater Adv Technol 151(1):60–64
87. Xu X, Jia J, Yang X, Dong S (2010) A templateless, surfactantless, simple electrochemical route to a dendritic gold nanostructure and its application to oxygen reduction. Langmuir 26(10):7627–7631
88. Jena BK, Raj CR (2007) Synthesis of flower-like gold nanoparticles and their electrocatalytic activity towards the oxidation of methanol and the reduction of oxygen. Langmuir 23(7):4064–4070
89. Jena BK, Raj CR (2007) Shape-controlled synthesis of gold nanoprism and nanoperiwinkles with pronounced electrocatalytic activity. J Phys Chem C 111(42):15146–15153
90. Kuai L, Geng B, Wang S, Zhao Y, Luo Y, Jiang H (2011) Silver and gold icosahedra: one-pot water-based synthesis and their superior performance in the electrocatalysis for oxygen reduction reactions in alkaline media. Chemistry 17(12):3482–3489
91. Seo B, Choi S, Kim J (2011) Simple electrochemical deposition of Au nanoplates from Au(I) cyanide complexes and their electrocatalytic activities. ACS Appl Mater Interfaces 3(2):441–446
92. Das AK, Raj CR (2011) Rapid room temperature synthesis of electrocatalytically active Au nanostructures. J Colloid Interface Sci 353(2):506–511
93. Plowman BJ, O'Mullane AP, Bhargava SK (2011) The active site behaviour of electrochemically synthesised gold nanomaterials. Faraday Discuss 152:43–62
94. Shim JH, Kim J, Lee C, Lee Y (2010) Electrocatalytic activity of gold and gold nanoparticles Improved by electrochemical pretreatment. J Phys Chem C 115(1):305–309
95. Chen D-J, Xu B, Sun S-G, Tong YJ (2012) Electroless deposition of ultrathin Au film for surface enhanced in situ spectroelectrochemistry and reaction-driven surface reconstruction for oxygen reduction reaction. Catal Today 182(1):46–53